Energy Profile and Transverse Single Particle Stability in Proton Linear Accelerators

V. Ziemann

Department of Physics and Astronomy
Uppsala University, Uppsala, Sweden

Draft of October 8, 2009

Abstract

We discuss the phase and energy margins for beam stability in linear proton accelerators.

1   Introduction

The beam stability in high power proton linacs such as the ESS [1] or the SPL [2] is of paramount importance, because even small losses will cause a high dose to the exposed areas and will make hands-on maintenance impossible. S. Peggs conjectured that some of the losses might be due to the loss of transverse stability if the phases of the linac are set to incorrect values. In this case the energy profile of the beam might not be compatible with the strength of the quadrupoles which are responsible for the transverse containment of the beam. In this report we will construct a simple model to investigate this field and use it to investigate the beam stability.

We start by considering a simple model linac that is sketched in Fig. 1 where the beam travels from right to left. We assume that the acceleration only happens in localized structures identified by the thick vertical bars in the figure. In each cavity the particle receives a maximum acceleration $\Delta\gamma = g_i \cos(\phi_i - \psi_i)$, where γ is the energy of the proton in units of its rest mass, psi_i is the phase of the cavity number i and $\phi_i = \omega\tau_i$ is the arrival phase of the particle at cavity i. Note that the cavity is characterized by its energy gain g and phase ψ whereas a beam particle is characterized by γ and $\phi = \omega\tau$. For convenience we assume that we know the beam phase ϕ_i just upstream of cavity i and the beam energy just after the cavity. The initial energy and phase of the beam are denoted by γ_0 and $\phi_0 = \phi_1$. The distance between the cavities is assumed to have a length L which is the same all along the linac. In this distance between the point-like cavities we
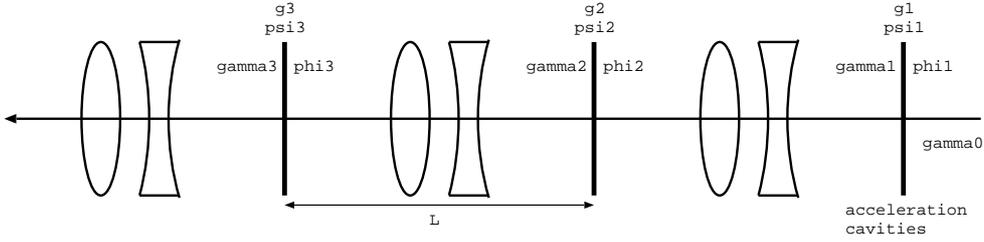
Figure 1: The schematic layout of the model linac used in this report.

have a single quadrupole doublet that is responsible for transversely focusing the beam. The resulting beta functions are shown in Fig. 2. In this example the focal length of the quadrupoles is $f = 2\,\mathrm{m}$ resulting in a phase advance of $97.2\,\mathrm{degree}$, which we use for the remainder of this report unless otherwise noted. We chose to use a rather strongly focusing lattice, because that should be more susceptible instabilities if the beam energy should be not matched to the lattice.

2   Simulation model

The simulation of such a simple system is quite straightforward. We first need to successively calculate the energy and phase of the beam at every cavity. Knowing the arrival phase ϕ_i yields the energy gain $\Delta\gamma_i = \gamma_i - \gamma_{i-1} = g_i\cos(\phi_i - \psi_i)$ which in turn yields the energy γ_i after the cavity. Knowing the energy yields the velocity of the particle $\beta_i = v_i/c = \sqrt{1 - 1/\gamma_i^2}$ which in turn determines the arrival time at the next cavity $t_{i+1} = L/v_i$ which, multiplied by the cavity frequency ω yields the arrival phase $\phi_{i+1} = \omega L/c\sqrt{1 - 1/\gamma_i^2}$. In this way the map of ϕ_i, γ_i to ϕ_{i+1}, γ_{i+1} can be constructed. Explicitly it can be written as

$$
\begin{aligned}
\phi_{i+1} &= \phi_i + \frac{\omega L/c}{\sqrt{1 - 1/\gamma_i^2}} \\
\gamma_{i+1} &= \gamma_i + g_i\cos(\phi_i - \psi_i)
\end{aligned}
\tag{1}
$$

and is easily coded in Matlab [3].

Finding the cavity phase ψ_i that yield the maximum energy gain is achieved by requiring that the cavity phase ψ_i is equal to the arrival phase of the beam ϕ_i. In that case the argument of the cosine is zero, resulting in the maximum gain $\Delta\gamma = g_i$ which also means that the beam is accelerated on-crest of the RF. Normally one chooses to operate the linac at a different phase, because of phase stability. In that case we adjust all phases to whatever off-crest phase is desired. The following excerpt of Matlab code exemplifies this
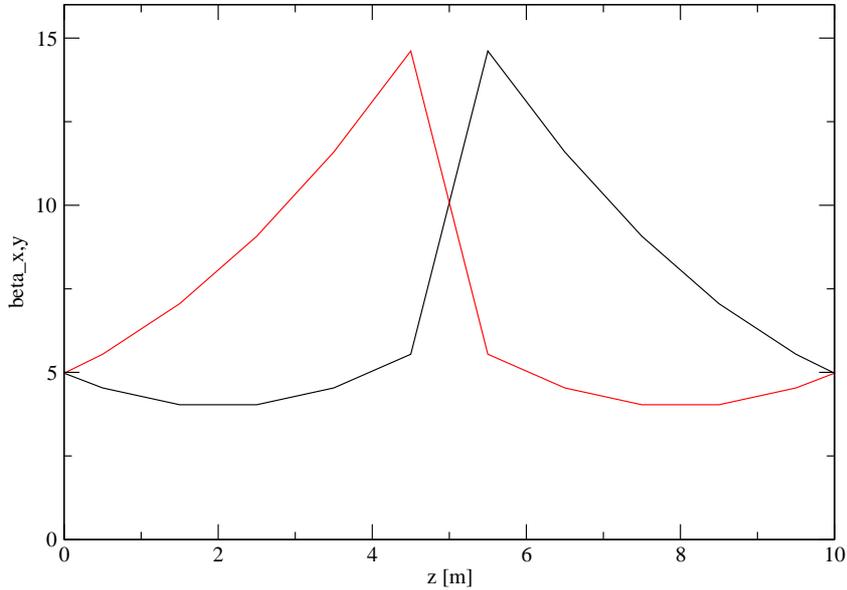
```
psi(1)=-dpsi;
```

2

Figure 2: The horizontal and vertical beta functions between the cavities. The focal length of the thin lens quadrupoles is assumed to be $f = 2\,\mathrm{m}$ giving a phase advance of 97.2 degree.

```
gamma(1)=gstart+g(1)*cos(phi(1)-psi(1));
for k=2:ncell
    phi(k)=phi(k-1)+(omega*L/c)/sqrt(1-1/gamma(k-1)^2);
    phi(k)=rem(phi(k),2*pi);
    psi(k)=phi(k)-dpsi;
    gamma(k)=gamma(k-1)+g(k)*cos(phi(k)-psi(k));
end
```

where `dpsi` is the desired phase offset.

Once the energy profile γ_i is known along the linac we can calculate how it varies if for example the initial energy of the beam γ_0 or the arrival phase ϕ_0 are varied. We will discuss this further below.

The transverse stability of the beam can be investigated by calculating the transfer matrix of a section between cavities and see how it varies with the energy. We observe that the transfer matrix R of the doublet cell is given by

$$R \;=\; \begin{pmatrix} 1 & l \\ 0 & 1 \end{pmatrix} \begin{pmatrix} 1 & 0 \\ -1/f & 1 \end{pmatrix} \begin{pmatrix} 1 & l_2 \\ 0 & 1 \end{pmatrix} \begin{pmatrix} 1 & 0 \\ 1/f & 1 \end{pmatrix} \begin{pmatrix} 1 & l \\ 0 & 1 \end{pmatrix}$$
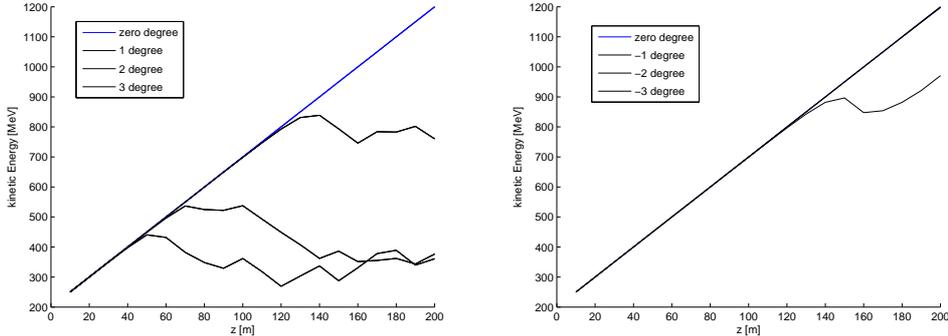
3

Figure 3: The energy profile along the linac with initial arrival phase errors of 0, 1, 2, and 3 degree (above) and 0, -1, -2, and -3 degree (below).

$$= \begin{pmatrix} 1 + l_2/f - l_2l/f^2 & 2l + l_2 - l_2l^2/f^2 \\ -l_2/f^2 & 1 - l_2/f - l_2l/f^2 \end{pmatrix} \tag{2}$$

where l is the drift space from the cavity to the adjacent quad and l_2 the distance between the quadrupoles which have a default focal length f at the design energy profile which is specified by the procedure elaborated before. If the beam energy at the quadrupoles is different, say $\bar{\gamma}$, we can simply scale the focal length by the ratio of the momenta at the respective energies or, equivalently, by $\beta\gamma = \sqrt{\gamma^2 - 1}$.

The single-particle transverse stability of the entire linac is then determined by the trace of the product of all transfer matrices along the linac, evaluated at the real beam energy, rather than the design energy. If the trace of the cumulative transfer matrix is below or equal to 2 the beam is stable, if it exceeds 2 the beam is unstable.

3   On-crest operation

We now use the model to explore simple configurations and their respective stability. We start by considering on-crest operation, where the arrival phase is adjusted to coincide with the maximum acceleration gradient and therefore results in the highest final energy. Fig. 3 shows such the energy profile along the length of the linac z for three different positive arrival phases $\phi_0 = 0, 1, 2, 3$ degree. We observe that only the beam with the correct phase zero reaches the maximum energy and the other three phases result in considerably lower final energies. We also note that during the first few meters there is only a very small effect, but once the energy is lower, it never really recovers and only meanders around the energy where the problem first appears. When starting with negative phases ϕ_0 the situation is slightly better, for a phase offset of up to 2 degrees no degradation
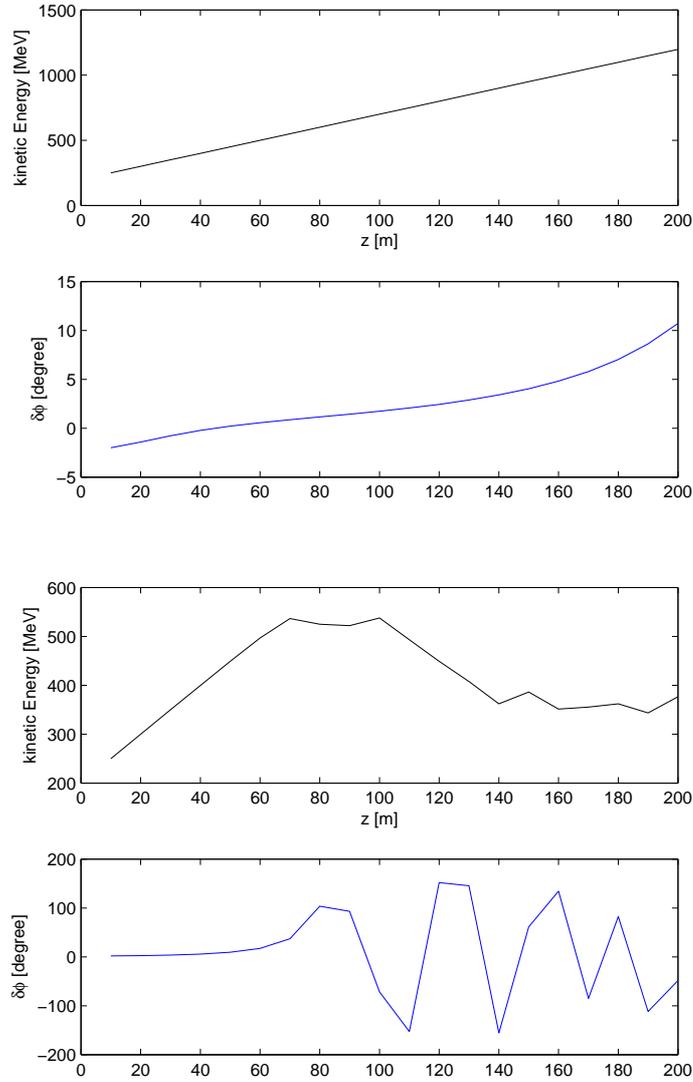
4

Figure 4: The energy profile along the length of the linac with an initial phase error of -2 degree (above) and +2 degree (below).
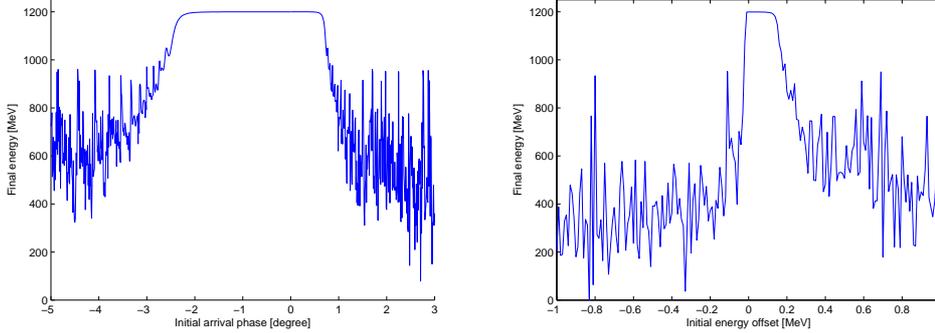
Figure 5: The energy at the end of the linac as a function of the initial phase offset (left) and offset in kinetic energy (right).

of the final energy is visible on the bottom graph of Fig. 3, only for -3 degrees the energy profile deteriorates.

In order to understand this asymmetry between positive and negative phases we display both the energy and the phase difference of the beam phase and the cavity phase $\phi_i - \psi_i$ in Fig. 4 for an initial phase offset of -2 degrees in the upper graph and +2 degrees in the lower graph. We see that the negative initial phase offset leads to a much smoother phase variation with a magnitude of only a few degrees, whereas the positive phase offset leads to much larger phase oscillations leading to both acceleration and deceleration, which results in the meandering energy profile.

The physics behind this observation is quite simple. If the initial arrival phase is negative, the beam arrives too early and and also receives an energy gain that is too low. Since it is too early the time to reach the next cavity down the line is longer, which is also accomplished because the energy and consequently also the velocity is lower. Both effects of *too early* and *too little energy* thus compensate one another in the case of negative phase offset, but add in the case of positive offset. Of course this is only true when operating on-crest, because one operates at the phase giving the maximum energy gain.

In order to investigate the stability more quantitatively, we repeated the above analysis and calculate the final energy while varying the incoming phase ϕ_0 and energy γ_0 and display the result in Fig. 5. We see that the bandwidth is on the order of two degree in phase, which is consistent with the previous observation discussed in relation with Fig. 3. The energy bandwidth is less than $0.2\,\mathrm{MeV}$ which is on the order of 10^{-3} of the starting energy which is assumed to be $200\,\mathrm{MeV}$. But this is a consequence of accelerating on-crest, a restriction, that we will drop in the next section.

In Fig. 6 we display the figure of merit for transverse stability $\max(\mathrm{Tr}(R(z)))$ that we introduced near the end of section 2 as a function of the initial phase
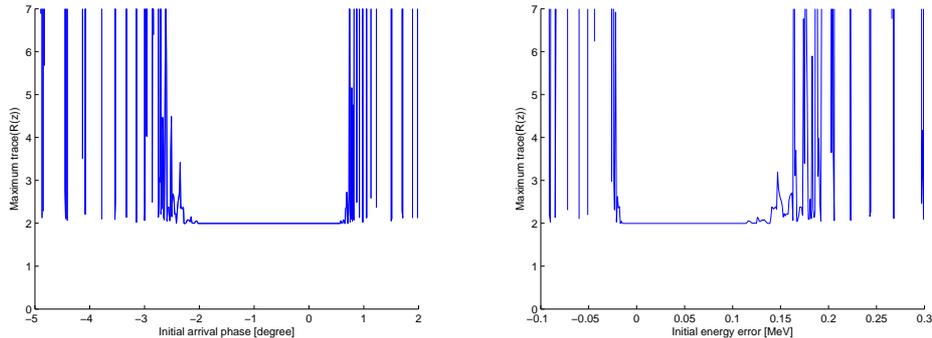
6

Figure 6: The maximum of $\mathrm{Tr}(R(z))$ along the length of the linac as a function of the arrival phase (left) and the arrival energy (right).

error ϕ_0 and initial energy error $\Delta\gamma_0$. If the stability parameter is less or equal to 2, the transverse motion is stable, which is the case for the same range as the bandwidth determined from the maximum achievable energy, displayed in Fig. 5. We conclude that, at least for on-crest operation, the bandwidth for the maximum achievable energy coincides with that of transverse stability. Conversely, if the initial phase and energy lie outside the energy bandwidth, also transverse stability cannot be guaranteed, which is intuitively clear, because if the maximum energy is not reached, the quadrupoles are mismatched to the beam energy, as discussed in section 2.

Having discussed on-crest operation, we now proceed and drop this restriction and consider off-crest operation. We start by determining the optimum phase in the next section.

4   Off-crest operation

Now we drop the restriction to operate on-crest to achieve the maximum final energy which has the consequence that just the final energy is lower. If all cavities are tuned to the same off-crest phase $\Delta\psi$ the final energy is lower by a factor $\eta = \cos(\Delta\psi)$, but we gain an improved stability margin. In Fig. 7 we show the bandwidth of transverse stability, defined by $\max(\mathrm{Tr}(R(z))) \leq 2$ as a function of the off-crest phase $\Delta\psi$ and observe that the bandwidth (blue) increases with more negative off-crest phase at the expense of the maximum achievable energy (green). For the following calculations we will use a phase of $\Delta\psi = -10$ degree, because it will only cause an energy reduction of about 1.5% and still has an energy bandwidth of more than $1\,\mathrm{MeV}$.

In order to illustrate the bandwidth calculation we show the bandwidth scan for $\Delta\psi = -10$ degree in the top two plots in Fig. 8. Again we see that the
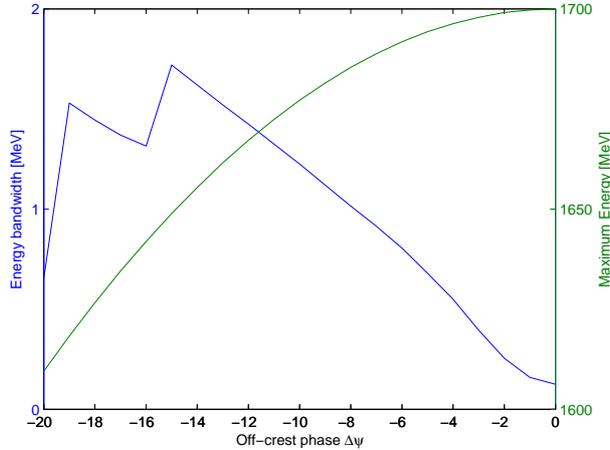
7

Figure 7: The energy bandwidth (blue) and the maximum achievable energy (green) as a function of the off-crest phase.

bandwidth determined from the transverse stability parameter (above) coincides with that of the maximum energy (below). In Fig. 9 we display the bandwidth with respect to the initial phase ϕ_0 for an off-crest phase of -10 degree. Here the bandwidth extends from about -5 degree to about 20 degree for a total of 25.15 degree as is stated on the graph. Note, that the bandwidth of the transverse stability (upper plot) and the final energy E_{max} (lower) coincide, leading to the observation the "if the energy is right, transverse stability follows suit."

5   Cavity Phase Tolerances

So far we have determined the bandwidth with respect to the tolerable variation in the initial energy and phase offset of which the latter is equivalent to a phase error of the first cavity. One might therefore ask how the phase bandwidth varies for all the other cavities along the linac. Intuitively we expect that the phase errors are less severe further down the linac, where the beam energy is higher and an error in energy causes less velocity variation, which in turn would lead to even larger phase errors downstream. We investigate this susceptibility of the beam stability and final energy with respect to phase errors by first calculating the proper phases that will give a constant off-crest phase at all cavities and then change one cavity at a time by ± 3 and ± 10 degrees and calculate the bandwidth with respect to the initial phase offset ϕ_0, i.e. we produce a plot similar to the one in Fig. 9, but with one cavity at a time de-phased and show the result in Fig. 10.

In the left plot in Fig. 10 we observe that the positive phases lead to lower
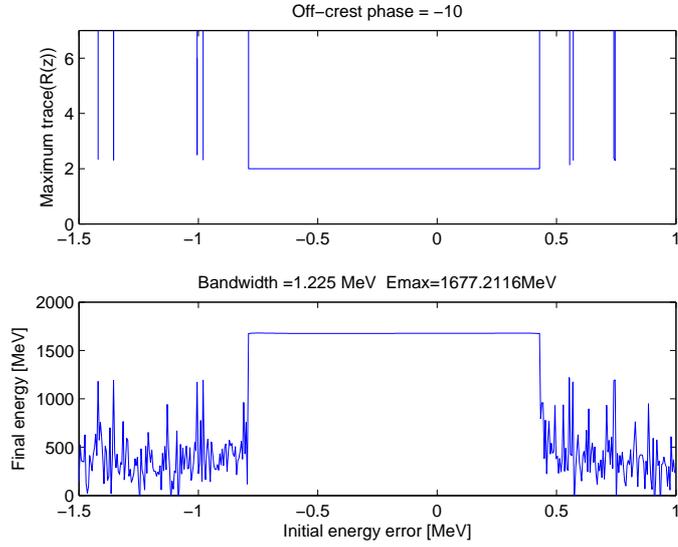
8

Figure 8: The maximum of $\text{Tr}(R(z))$ and the maximum achievable energy E_{max} along the length of the linac as a function of the arrival energy when the linac operates with -10 degree off-crest phase.
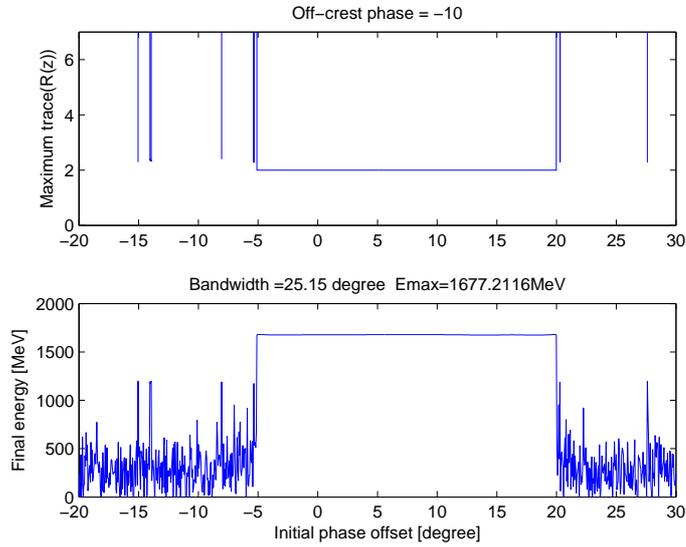

Figure 9: $\text{Max}(\text{Tr}(R(z)))$ and E_{max} along the length of the linac as a function of the arrival phase when operating at $\Delta\psi = -10$ degrees.
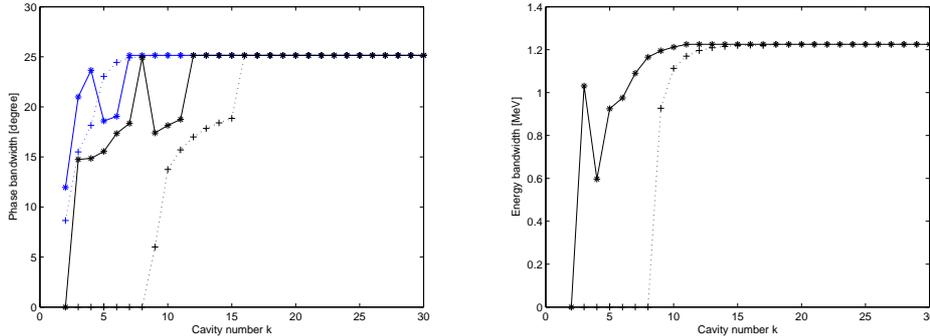
Figure 10: The left plot shows the phase bandwidth of the linac if cavity number k is detuned by $+3$ degree (blue dots), -3 degree (solid blue), $+10$ degree (black dots), and -10 degree (solid black). The bandwidth of the unperturbed linac is given in Fig. 9 to be 25.15 degree. Furthermore, if the bandwidth is zero, the linac is unstable. The right plot shows the corresponding energy bandwidth for ± 10 degree approaching the unperturbed value of 1.225 MeV shown in Fig. 8.

bandwidth and are consequently disadvantageous. We also observe that the cavities further downstream than half-way down the linac are less susceptible and even a 10 degree error with either sign, does not cause a deterioration of the phase bandwidth. The right plot in Fig. 10 shows the energy bandwidth corresponding to what is shown in Fig. 8 for one cavity at a time detuned by ± 10 degrees. Again, we find that about half-way down the linac errors on the order of 10 degree do not affect the bandwidth any more.

When running all the individual simulations leading to Fig. 10 we observed that in some cases $\max(\text{Tr}(R(z)))$ was well-behaved and stayed below or equal to 2, while the maximum energy actually exhibited a dip in the maximum achievable energy, which is shown in Fig. 11. At about -0.5 MeV initial energy offset the maximum reachable energy is considerably lower by more than 100 MeV. If the initial beam has a wide distribution in energies this will lead to a low energy tail that extends to very low energies. One conclusion we can reach from this observation is that the transverse stability is less susceptible to energy errors than the final energy.

We investigate the dip closer by generating plots with the kinetic energy $T(z)$, the phase $\phi(z)$ and transverse stability $Tr(R(z))$. We also generate plots of longitudinal phase space where we display the deviation of the kinetic energy $\Delta T = T - T_0$ against the phase ϕ. Here T is the kinetic energy and T_0 that of the design configuration. We choose a point to the right of the dip at $\Delta T = -0.4$ MeV, in the middle of the dip at $\Delta T = -0.55$ MeV and to the left of the dip at $\Delta T = -0.7$ MeV. The resulting plots are shown in Fig. 12. Note that the starting point atcavity 1 is identified by a red asterisk. We observe that
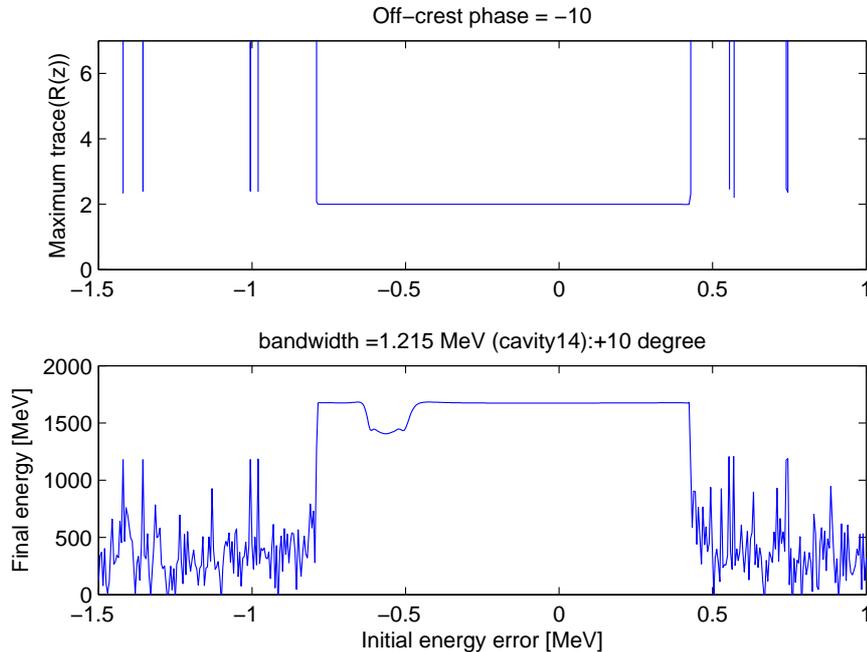
Figure 11: The transverse stability bandwidth of the linac operating at -10 degrees off-crest when cavity 14 is tuned to 0 degrees which means it operates on-crest. The stability bandwidth is determined from the $\text{Tr}(R(z))$ plot. Note that the maximum achievable energy in the lower graph has a pronounced dip at an energy offset of -0.5 MeV. This would cause part of the beam that has this offset to develop a tail with very low energy.

the phase space of the center row which describes a configuration inside the dip, differs from the top and bottom row which describe configurations outside the dip by showing synchrotron oscillations with an amplitude of a few MeV, whereas the center in-dip phase space is unbounded and the particle swirls down towards lower energies. This is also visible on the upper subplot of the left plot in the center row, that displays the energy along the linac, which deviates from a linear increase near $z = 250\,\text{m}$. We also see that the corresponding phase starts to oscillate. It looks like the qualitative difference comes from the particle 'jumping out of the bucket'.

6   Random Phase Errors

In order to determine the accuracy to which the phases along the linac have to be set we introduced uniformly distributed random phase errors to the phases of the cavities and calculated the energy and phase bandwidth for ten seeds each. The
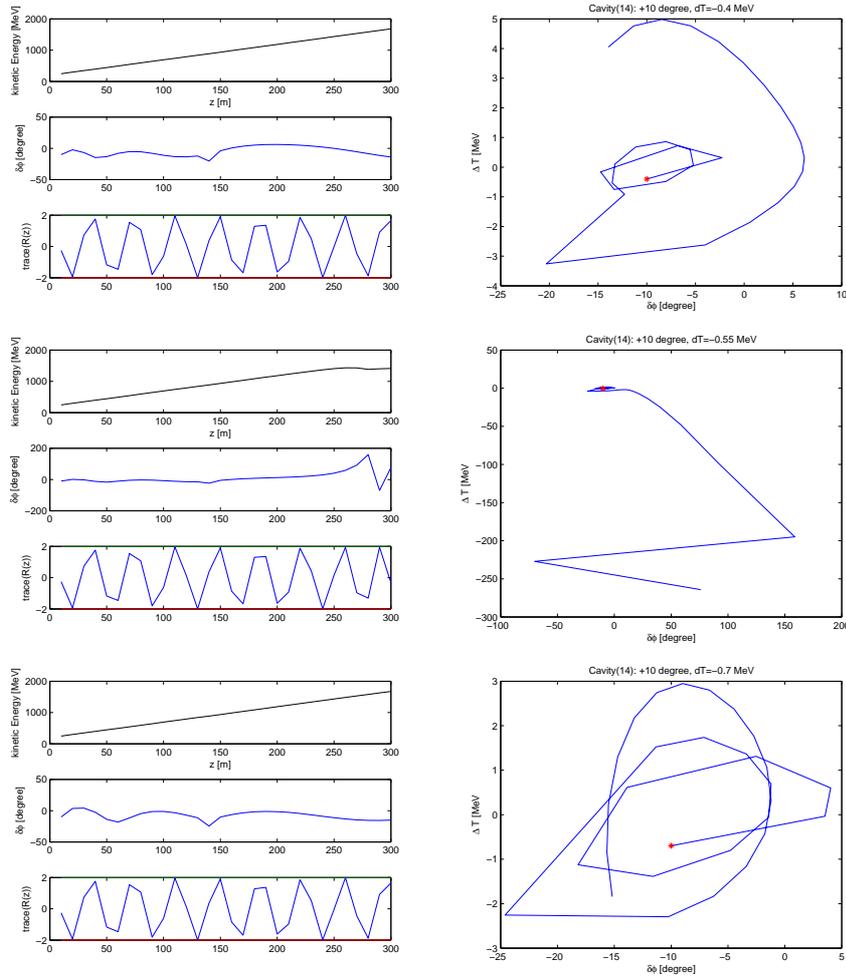
Figure 12: Investigating the dip by showing the energy, phases and $Tr(R(z))$ (left) and the phase space (right) corresponding to Fig. 11 with initial energy offset of -0.4 MeV (top row), -0.55 MeV (middle row), and -0.7 MeV (bottom row).
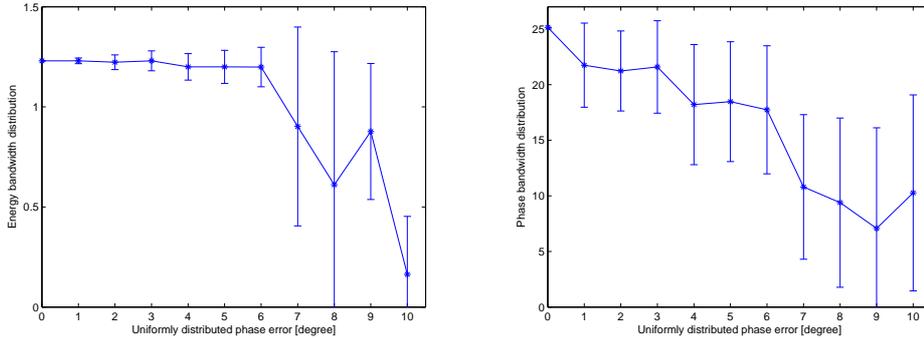
12

Figure 13: The variation of the energy bandwidth (left) and phase bandwidth (right) as a function of uniformly distributed random phase errors of the cavities.

applied phases errors are distributed in the interval $[-\Delta\phi/2, \Delta\phi/2]$ where $\Delta\phi$ is varied between 0 and 10 degree. The average and rms spread of the bandwith values over the ten seeds are depicted in Fig. 13 as a function of $\Delta\phi$. We find that the energy bandwidth shown on the left has a distinct drop accompanied by a significant increase in the spread as shown by the error bar after $\Delta\phi = 6$ degrees. This would imply that the phases of the linac should be set within a practical error window of about 5 or 6 degrees. The corresponding phase bandwidth which is shown on the right in Fig. 13 does not show this as succinctly, but still therealso is a significant drop in the phase bandwidth between 6 and 7 degree phase errors, such that we interpret this as corroborating evidence for the phase window of 5 to 6 degree.

7 Transverse phase advance

In all of the previous investigations we used a focal length of $f = 2\,\text{m}$ in the doublet cells between the cavities resulting in phase advance of 97 degree per cell. Now we will vary the focal length between $f = 1.5\,\text{m}$ which yields a phase advance of 180 degree and $f = 20\,\text{m}$ which yields a phase advance of 8.6 degree per cell.

In order to assess the transverse stability we calculate both the energy and phase bandwidth, such as is shown in Fig. 8 and 9 and see how the beandwidth varies with the focal length used in the doublet lattice. It turned out,however, that *the bandwidth almost did not change at all.* For all of the 15 different tested values the reported energy bandwidth was 1.225 MeV and the phase bandwidth 25.15 degree. There was one exception at $f = 3\,\text{m}$ which corresponds to a transverse phase advance of 60 degee per cell for which the bandwidth was considerbly smaller. If the focal length, on he other han, was chosen to be slighly different
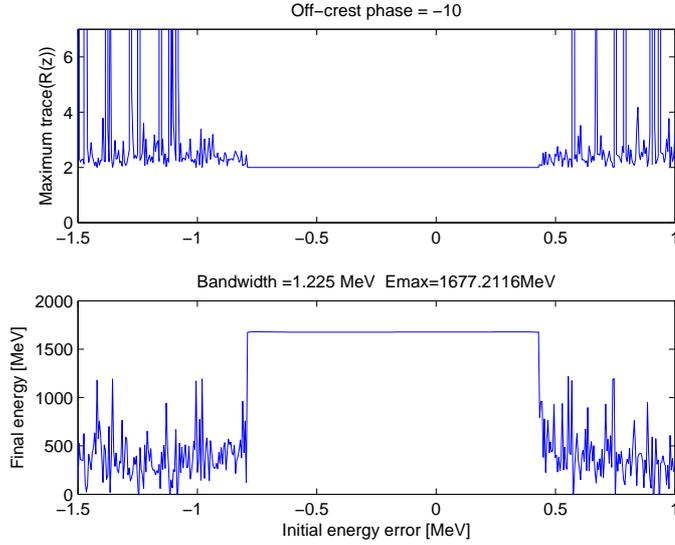
13

Figure 14: The energy bandwidth with a lattice where the focal length is chosen to be $f = 15$ m resulting in a weak transverse phase advance of 11.5 degree. Note that c, compared to Fig. 8 $Tr(R)$ does not grow as quickly adjacent to the borders of stability at ± 0.4 MeV.

from 3 m the bandwidth was unaffected. This behaviour is probably due to the fact that even the unperturbed lattice is close to the stability limit $Tr(R^3) = 2$ and a small change in the energy can tip the system over the stability thershold. The same observation is also true for the 180 degree case with $f = 1.5$ m. It appears that it is advisable to stay away from all to rational phase advances, just as in circular machines.

In Fig. 14 we show the energy bandwidth plot for a focal length of $f = 15$ m. We observe that the weak phase advance causes $Tr(R)$ in the upper plot to differ only weakly adjacent to the limit of stability at ± 0.4 MeV compared to Fig. 8 where the quadrupoles are much stronger. There the limit of transverse stability is much sharper.

We interpret the insensitivity of the bandwidths with respect to the focal length, or equivalently, the phase advance as an indication that the transverse stability is *not the primary cause* of beam loss. On the other hand, it is obvious that a significant energy mismatch will cause a loss of transverse stability as a secondary effect.

8   Conclusions

We investigated the stability of a proton linac using a very simple model shown in Fig. 1 and characterized it in terms of bandwidth of the maximum achievable energy and the transverse stability parameter. We found that the energy bandwidth and the transverse stability bandwidth are closely correlated as is witnessed by Figs. 8 and 9. In the course of the investigation we also confirmed increased beam stability and bandwidth at the expense of achievable maximum energy by moving the beam off-crest. We established that random phase errors on the order of about 5 degree are managable.

References

[1] S. Peggs, et al., *Conceptual design of the ESS-SCANDINAVIA,* Presented at the Particle Accelerator Conference PAC 09 in Vancouver, BC, Canada, May 2009.

[2] F. Gerigk (editor), *Conceptual Design of the SPL II,* CERN Yellow Report CERN-2006-006.

[3] `http://www.mathworks.com`